Earth Syst. Sci. Data Discuss., 7, 59–88, 2014
www.earth-syst-sci-data-discuss.net/7/59/2014/
doi:10.5194/essdd-7-59-2014


Open Access Earth System Science Data Discussions



# A global climatology of total columnar water vapour from SSM/I and MERIS

**R. Lindstrot[1], M. Stengel[2], M. Schröder[2], J. Fischer[1], R. Preusker[1], N. Schneider[2], and T. Steenbergen[2]**

[1]Institut für Weltraumwissenschaften, Freie Universität Berlin, Carl-Heinrich-Becker-Weg 6–10, 12165 Berlin, Germany
[2]Deutscher Wetterdienst, Satellite-Based Climate Monitoring, Dept. Climate and Environment, Strahlenbergerstraße 13, 63067 Offenbach, Germany

Received: 18 December 2013 – Accepted: 20 December 2013 – Published: 24 January 2014

Correspondence to: R. Lindstrot (rasmus.lindstrot@wew.fu-berlin.de)

Published by Copernicus Publications.







## Abstract

A global time series of total columnar water vapour from combined data of the Medium Resolution Imaging Spectrometer (MERIS) onboard ESA's Environmental Satellite (ENVISAT) and the Special Sensor Microwave/Imager (SSM/I) onboard the satellite series of the US Defense Meteorological Satellite Program (DMSP) is presented. The unique dataset, generated in the framework of the ESA Data User Element (DUE) GlobVapour project, combines atmospheric water vapour observations over land and ocean, derived from measurements in the near infrared and the microwave range, respectively. Daily composites and monthly means of total columnar water vapour are available as global maps on rectangular latitude-longitude grids with a spatial resolution of $0.05^\circ \times 0.05^\circ$ over land and $0.5^\circ \times 0.5^\circ$ over ocean for the years 2003 to 2008. The data is stored in NetCDF files and is fully compliant with the NetCDF Climate Forecast convention. Through the combination of high quality microwave observations and near infrared observations over ocean and land surfaces, respectively, the dataset provides global coverage. The combination of both products is carried out such that the individual properties of the microwave and near-infrared products, in particular their uncertainties, are not changed and therefore well defined. Due to the global coverage and the provided uncertainty estimates this data set is potentially of high value for climate research. The SSM/I-MERIS TCWV data set is freely available via the GlobVapour project web page with associated doi (doi:10.5676/DFE/WV_COMB/FP).

In this paper, the details of the dataset generation, i.e. the satellite data used, the retrieval techniques and merging approaches are presented. The derived level 3 products are compared to global radiosonde data from the GCOS upper air network (GUAN), showing a high agreement with a root mean square deviation of roughly 4.4 $\mathrm{kg\,m^{-2}}$ and a small wet bias well below 1 $\mathrm{kg\,m^{-2}}$. Furthermore, the data set is shown to be free of seasonal biases. The consistency of the MERIS and SSM/I retrievals is demonstrated by applying the MERIS retrieval to sun glint areas over ocean.





ESSDD

7, 59–88, 2014



## 1 Introduction

Water vapour is the most important greenhouse gas in the Earth atmosphere. It accounts for about 70 % of the total atmospheric absorption of radiation and 60 % of the total natural greenhouse effect in clear sky cases (Kiehl and Trenberth, 1997; Trenberth et al., 2008). Water vapour is at the same time highly variable in space and time, as it is constantly brought into the atmosphere by evaporation, transported by advection and convection and depleted by condensation and precipitation. These mechanisms result in both horizontal and vertical transport of latent heat, dominating the structure of tropospheric diabatic heating (Trenberth and Stepaniak, 2003a, b). In recent years, an increase of tropospheric water vapour of about 1.2 % per decade was observed (Trenberth et al., 2005, 2007) in response to the observed increase of global surface temperatures. The water vapour feedback, i.e. the enhanced greenhouse effect due to increased humidity as a response to higher temperatures, is nowadays believed to be a comparatively strong and positive effect (e.g. Soden et al., 2002; Forster and Collins, 2004). Over the oceans, the absolute humidity in the lower atmosphere is closely linked to the near surface air temperature, i.e., the water vapour changes at roughly the same rate as the saturated vapour pressure, as estimated from the Clausius–Clapeyron law (see e.g. O'Gorman and Muller, 2010). The situation over the land masses is more complicated. Here, the limited supply of water available for evaporation results in an overall weaker but regionally varying feedback.

Accurate, long-term measurements of the global total column of water vapour (hereafter referred to as TCWV) are needed to fully understand and monitor these spatial and temporal variations and feedback mechanisms of water vapour. Satellite measurements of TCWV have the potential to provide the needed temporal and spatial coverage and resolution as well as retrieval accuracy to serve these purposes.

A variety of techniques for the retrieval of TCWV from satellite data have been developed during the past decades. Above the global oceans, microwave observations provide reliable information on total column water vapour. Due to the comparably low





ESSDD
7, 59–88, 2014



emissivity of water surfaces in the microwave region, the variability of the top of atmosphere microwave signal is dominated by the emission by water in its gaseous and liquid phase in the atmosphere. A number of different microwave sensors, such as NASA's Advanced Microwave Scanning Radiometer for EOS (AMSR-E) and Advanced Microwave Sounding Unit (AMSU) or the Microwave Humidity Sounder (MHS) instruments, deployed on a variety of operational polar orbiting satellites, are thus commonly used to measure profiles of water vapour as well as its vertical integral over the open ocean and assimilate the measurements for Numerical Weather Prediction (NWP) models. The longest available time series of microwave humidity observations is provided by the measurements of the SSM/I instrument series onboard the DMSP satellites. Data from SSM/I-type instruments is available starting from 1987 and is currently foreseen to be extended into the 2020s and even the 2030s through the DMSP programme and the EUMETSAT Polar System–Second Generation (EPS-SG), respectively, making it a valuable source for the generation of Climate Data Records (CDRs).

Above land and sea ice, microwave measurements are affected by large and highly variable surface emissivities. In the infrared, the limited knowledge of the skin temperature and the emissivity of land surfaces results in high uncertainties of the water vapour amount in the lower troposphere, where the bulk of the vertically integrated water vapour amount is present. However, hyperspectral sounders such as IASI (e.g. Pougatchev et al., 2009) and AIRS (e.g. Susskind et al., 2003), provide valuable information on the vertical humidity profile down to a level close to the surface. The integral of the vertical column of water vapour is best represented when using Differential Optical Absorption Spectroscopy (DOAS) in the near infrared or visible range. In contrast to infrared and microwave retrievals, here the information about TCWV is not carried by the thermal emission of the water vapour itself, but by the absorption of solar radiation in spectral regions of water vapour absorption. Exploiting Beer's law, the water vapour column amount can be deduced from the transmittance, which is approximated by the ratio of an absorbing channel inside the absorption band and a spectrally close channel outside of the absorption band. Moderately to highly reflective surfaces, such as





ESSDD
7, 59–88, 2014



most land surface types in the near infrared region, provide a high sensitivity to TCWV of such measurements. Over the dark ocean, this technique is not appropriate for the retrieval of TCWV.

Since spaceborne observations of TCWV with global coverage and high quality are hard to get from a single instrument type alone, it is indicated to use a combination of data sources to combine the strengths of the individual instruments. This strategy was successfully pursued by the Global Water Vapour Project (GVaP), which completed a successful pilot phase and developed a global water vapour data set (NASA Water Vapour Project, NVAP, Randel et al., 1996) from a combination of microwave and infrared sensors and radiosondes. A reanalysis and extension of NVAP, NVAP-M as part of the NASA-MEaSUREs program, was conducted in recent years and resulted in a 22 yr-spanning climatology of total and layered humidity (Vonder Haar et al., 2012).

In the frame of the ESA DUE GlobVapour project, a related approach was pursued by combining measurement of the Medium Resolution Imaging Spectrometer (MERIS) and SSM/I. MERIS measurements were used to derive TCWV over land and coastal ocean, complemented by SSM/I observations over ocean to achieve global coverage at comparably high quality.

The GlobVapour project combined SSM/I-MERIS dataset, comprised of global maps of daily composites and monthly means, is thus a unique combination of water vapour observations over land and ocean. Over land, the high spatial resolution of MERIS enables the generation of the products on a rectangular longitude-latitude grid with $0.05^{\circ} \times 0.05^{\circ}$ resolution. Over ocean, a $0.5^{\circ} \times 0.5^{\circ}$ resolution is provided. The data set in its current version ranges from 2003 throughout 2008 and is foreseen to be extended to cover at least the full mission lifetime of MERIS, which ended in April 2012. The data is provided in NetCDF format via the project website (www.globvapour.info) and is fully compliant with the NetCDF Climate Forecast convention.

In the following sections, the data set is presented in detail, covering a description of the instruments as well as the input data versions used (Sect. 2). The individual retrieval





ESSDD
7, 59–88, 2014



techniques are described in Sect. 3, while the merged data set and its validation are covered in Sects. 4 and 5, respectively.

## 2 Instrumentation and data provenance

### 2.1 The MERIS instrument

MERIS is a programmable, medium-spectral resolution, imaging spectrometer (Rast et al., 1999). It is one of ten core instruments on the polar orbiter ENVISAT (Environmental Satellite, launched on 1 March 2002) flying at 800 km in a sun-synchronous orbit with an equator crossing time of 10:00 a.m., ascending node, and 98.5° inclination. MERIS consists of 5 identical pushbroom imaging spectrometers, operating in the solar spectral range (390 to 1040 nm), arranged in a fan shape configuration which covers a total field of view of 68.5° and spans a swath width of around 1150 km. The spectral dispersion is achieved by mapping the entrance slit of a grating spectrometer onto a CCD array. The integration time, instrument optics and CCD array resolution are adjusted such that MERIS has a spatial resolution of 260 m × 300 m and a spectral sampling of 1.25 nm. The instrument electronic data rate provides 15 channels which are programmable by ground command in width and in position. In the regular operation mode the spatial resolution is reduced by a factor of 4 along and across track ("reduced resolution" mode). In the "full resolution" mode, the full spatial resolution is transmitted. MERIS data of the 3rd reprocessing of the Level 1 archive was used for the generation of the water vapour fields. Compared to previous reprocessings of the MERIS archive, a new calibration and improved geolocation had the most important impacts on the Level 1 products in terms of radiometry, geometry and flags for land/ocean/coastline classification (MERIS Quality Working Group, 2011).





ESSDD
7, 59–88, 2014



## 2.2 The SSM/I instrument

The SSM/I (Hollinger, 1991) is a passive, seven-channel, four-frequency microwave radiometer which is operated within the DMSP satellite series, flying on sun-synchronous orbits at an altitude of 830 km. The SSM/I is a conical scanner with a scan angle (satellite view angle with respect to nadir) of 45° which corresponds to an earth incidence angle of 53°. The four bands at 19 GHz, 22 GHz, 37 GHz and 85 GHz have dual polarisation except the 22 GHz channel, resulting in seven channels. Depending on the channel, SSM/I has a footprint of a few tens of kilometres. The first SSM/I instrument was carried by the F08 satellite, launched in 1987, the last one was launched on F15 in December 1999. The SSM/I was replaced by the SSMIS (Special Sensor Microwave Imager/Sounder) starting from DMSP satellite F16. The available long-term data record of SSM/I observations together with its high sensitivity to atmospheric water vapour makes it a very valuable source for climate studies. The generation of the TCWV fields was based on inter-calibrated SSM/I brightness temperatures of the F13 and F14 DMSP satellites (Andersson et al., 2010).

The data was provided by CM SAF as an early release of the CM SAF SSM/I FCDR edition 1.

SSM/I has been and is used in various applications for the retrieval of atmospheric water vapour using physical (e.g. Phalippou, 1996) and semi-physical schemes based on a statistical interpretation of a training dataset (e.g. Alishouse et al., 1990; Schlüssel and Emery, 1990; Schulz et al., 1993; Wentz, 1997).

# 3 Retrieval techniques

## 3.1 TCWV retrieval over land and coastal ocean using MERIS

The MERIS scheme for the retrieval of TCWV makes use of the differential absorption of solar radiation by atmospheric water vapour in the near infrared spectral range.





ESSDD
7, 59–88, 2014



Since the retrieval is thus based on the analysis of surface-reflected solar radiation, the retrieval can only be applied during daytime and under clear sky conditions. Two channels of MERIS, located within and close-by the shortwave end of the $\rho\sigma\tau$-absorption band at 900 nm are used for the approximation of the water vapour transmittance. The measurements are sensitive to water vapour over moderately bright to bright underlying surfaces, such as almost all land surface types.

### 3.1.1 MERIS cloud screening

Due to the high albedo of clouds, the underlying atmosphere and the water vapour it contains are hidden to space-based observations in the near infrared. In cases of semitransparent clouds present in the field of view, a part of the radiation penetrates through the clouds while still a significant fraction is reflected at the cloud itself, causing a reduction of the observed water vapour absorption. A potential correction of these effects, taking into account the MERIS-derived cloud height and optical depth as well as the tabulated surface reflectance, would only be possible at the expense of strongly increased retrieval uncertainties. Moreover, the MERIS product would be deprived of its most important strength, the high sensitivity to variations in the boundary layer humidity. The first mandatory pre-processing step in the MERIS processing chain therefore is the screening of all clouds.

The cloud detection is realized by the utilization of one of four different artificial neural networks (ANN), depending on whether the measurement is taken over an ocean, land, snow or ice surface. The ANNs use the majority of MERIS spectral bands, including the oxygen A band channel that is sensitive to the presence of clouds and their height (e.g. Preusker and Lindstrot, 2009). In addition, the input to the ANNs are the observation geometry, the surface pressure and the central wavelength of the oxygen A band channel. The latter is needed to account for the variable spectral center wavelength of the absorption channel (Delwart et al., 2007; Lindstrot et al., 2010), while knowledge of the surface pressure is required to optimize the use of the pressure information carried by the oxygen absorption.





ESSDD
7, 59–88, 2014



The ANNs were trained with radiative transfer simulations of MERIS radiances, performed with the Matrix Operator Model (MOMO, Fell and Fischer, 2001; Hollstein and Fischer, 2012). The training data bases covered the complete range of observation conditions and geophysical conditions possible for each regime. The output of each ANN is the probability of cloudiness, ranging from 0 to 1.

After applying the ANNs, pixels exhibiting a cloud probability of larger than 0.2 were masked out. In order to exclude cloud edges, areas identified as cloudy were extended by additionally masking a zone of two MERIS pixels (≈ 2 km) surrounding each cloudy pixel.

### 3.1.2 MERIS water vapour retrieval

The TCWV retrieval itself is described in detail in Lindstrot et al. (2012). The algorithm is divided into two individual steps, starting with a determination of the surface reflectance in MERIS bands 14 at 885 nm (window channel) and 15 at 900 nm (absorption channel) and a subsequent iterative optimization of TCWV by minimizing the cost function, represented by the absolute difference between the modelled and observed ratios of MERIS bands 15 and 14.

After correcting the measured MERIS band ratio for differences in the surface reflectance between 885 nm and 900 nm, the forward simulation of the MERIS bands is based on a calculation of the water vapour absorption optical depths. These are calculated using an advanced $k$-distribution technique (Bennartz and Fischer, 2000) with the absorption line parameters extracted from the HITRAN2008 database (Rothman et al., 2009). The effects of temperature and pressure on the calculated optical depths are considered by using a digital elevation model and ERA Interim 2 m temperatures. This secondary correction of the absorption optical depth is the only influence of reanalysis data on the MERIS water vapour retrieval.

In order to account for the influence of scattering on the measured band ratio, a scattering correction factor is calculated from pre-calculated look-up tables at each retrieval iteration step. The cost function minimization is achieved by a simple secant method





ESSDD
7, 59–88, 2014



and is regarded successful as soon as the cost function falls below a pre-defined threshold. Except for the ERA Interim 2 m temperature algorithm does not rely on any sort of prior knowledge.

The uncertainty of the retrieved value of TCWV is calculated after the final iteration step, by taking into account uncertainties introduced by instrumental effects such as sensor noise and uncertainties in background knowledge of the influencing parameters such as surface albedo, aerosol optical depth, aerosol vertical distribution, temperature profile and surface pressure.

### 3.2 TCWV retrieval over ocean using SSM/I

(Semi-)statistical TCWV retrievals over oceans, based on recalibrated and homogenized radiance data records from SSM/I observations, are available from, e.g., Remote Sensing Systems (RSS – Wentz, 1997) and Satellite Application Facility on Climate Monitoring (CM SAF – Schlüssel and Emery, 1990; Andersson et al., 2010; Schröder et al., 2013). Here, the core of the algorithm used in the frame of the GlobVapour project to derive total column water vapour from SSM/I measurements is based on a one-dimensional variational retrieval (1D-Var) scheme developed at ECMWF (Phalippou, 1996). While the initial application of the scheme was for the SSMIS microwave imager/sounder and AMSU (Advanced Microwave Sounding Unit), it was further extended to be a stand-alone scheme also applicable to SSM/I (Deblonde, 2001) for utilisation in the Satellite Application Facility for Numerical Weather Prediction (NWP SAF). The scheme is used to derive TCWV from brightness temperatures of SSM/I over ice-free ocean. The best estimate of the atmospheric state, composed of atmospheric temperature, moisture and liquid cloud condensate as well as surface variables temperature and wind speed, is determined by an iterative adjustment of the state vector to match the simulated satellite radiances with the measurements. The term "best estimate" refers to the optimal estimation theory (Rodgers, 2000) and describes the state vector $\boldsymbol{x}$ that minimizes the cost function $J$ taking into account the errors in the





ESSDD
7, 59–88, 2014



background information **B** and in the measurement **R**:

$$J = 1/2(\boldsymbol{x} - \boldsymbol{x}_b)^T \mathbf{B}^{-1}(\boldsymbol{x} - \boldsymbol{x}_b) + 1/2(\boldsymbol{y} - H(\boldsymbol{x}))^T \mathbf{R}^{-1}(\boldsymbol{y} - H(\boldsymbol{x})) \quad (1)$$

$H$ denotes the observation operator (here based on radiative transfer calculations) and $\boldsymbol{y}$ the measurements. With this methodology, a retrieval uncertainty is calculated for each of the control vector elements. In this framework, the 1D-Var scheme uses ERA-Interim atmospheric and surface fields as background information, with the exception of the background information for water vapour, for which climatological averages are used.

## 4 Combined data set

In order to achieve a global time series of TCWV with high accuracy above both land and ocean, the retrievals of MERIS above land and SSM/I above ocean were combined to produce daily composites and monthly means on a rectangular longitude–latitude grid. Above land, the 1 km$^2$ resolution of the MERIS product enables a spatial resolution of 0.05° × 0.05°. Above ocean, the spatial resolution is 0.5° × 0.5° due to the larger footprint of SSM/I. The SSM/I and MERIS retrievals have reduced quality over coastal areas relative to the respective retrievals over ocean and land. The coastal areas are filled with MERIS-derived TCWV. Note that TCWV at coastal areas will have increased uncertainties. Due to the forenoon orbit of ENVISAT (equator crossing time at 10 a.m.) and the fact that the MERIS retrieval relies on measurements of the reflected solar radiation in the near infrared spectral range, the resulting time series over land is a cloud-free, forenoon climatology. In order to establish consistency between land and ocean, only morning measurements (descending swath) of SSM/I onboard the DMSP satellites F13 and F14 (equator crossing time between 6 a.m. and 8 a.m.) were used for the retrieval of TCWV over ocean. As microwave measurements of TCWV are possible under cloudy and clear-sky conditions, TCWV was calculated with and without cloud screening.





ESSDD
7, 59–88, 2014



### 4.1 Daily composites

The daily composites of TCWV combine the MERIS measurements above land and coastal ocean with the daytime measurements of descending SSM/I orbits over the open ocean. Over land and the coastal ocean, the content of each grid box is calculated from a weighted average of the contributing $n$ MERIS pixels, with the weight $w_i = 1/\sigma_i^{\mathrm{rel}2}$ of each contributing pixel defined by its relative uncertainty $\sigma_i^{\mathrm{rel}} = \sigma_i/\mathrm{TCWV}_i$ with $\sigma_i$ being the uncorrelated uncertainty:

$$\mathrm{TCWV} = \left(\sum_{i=1}^{n} w_i \mathrm{TCWV}_i\right) \Big/ \sum_{i=1}^{n} w_i \tag{2}$$

The number of MERIS pixels contributing to a grid box is up to 30 in the tropics and drops to 20 at 50° latitude and 10 at 70° latitude.

In case of purely random errors and thus for averaging $n$ measurements, the uncertainty $\sigma$ of the average value is

$$\sigma = 1 \Big/ \left(\sum_{i=1}^{n} 1/{\sigma_i}^2\right)^{1/2} \tag{3}$$

This results in a reduction of uncertainty if more measurements are averaged. However, within a grid box, the level 2 uncertainties of the contributing measurements can not be regarded as uncorrelated, since critical forward modelling assumptions, such as the aerosol type, will affect all individual measurements in the grid box in a correlated way. In order to account for this, a more conservative approach was taken by calculating the resulting grid box uncertainty as the average uncertainty of the contributing measurements:

$$\sigma = \sum_{i=1}^{n} \sigma_i/n \tag{4}$$





ESSDD
7, 59–88, 2014



Therefore, the uncertainty values provided for each daily composite grid box over land and coastal ocean provide an upper boundary of the uncertainty. In addition, the standard deviation of the contributing MERIS measurements is provided in each grid box as it provides information about the sub-grid variability of TCWV.

Over ocean, SSM/I TCWV retrievals are sampled per $0.5^{\circ} \times 0.5^{\circ}$ grid box together with the calculated retrieval uncertainty. These data are then oversampled by a factor of 10 in order to be combined with the MERIS data to provide a single data field containing both data sources. To enhance the usability of the combined SSM/I-MERIS data set, it is available with a reduced global resolution of $0.5^{\circ} \times 0.5^{\circ}$.

Figure 1 shows an example of a global SSM/I-MERIS daily composite of TCWV and its associated uncertainty (note the change of color scale). Over land, the smaller swath of MERIS and the limitation to clear sky scenes results in a lower coverage compared to the open ocean, observed by SSM/I, where only heavily precipitating regions are masked out. The number of single observations used for the generation of the daily composite values is shown in the bottom panels, with the number of MERIS observations used to fill each grid box varying between 0 and 30, while generally single SSM/I measurements were used over ocean.

Figure 2 shows a zoom into the Mediterranean Sea area for a daily composite from 2 May 2003. It shows a smooth transition of the water vapour field between land and ocean as well as a somewhat increased uncertainty in the coastal areas, where MERIS measurements are used to fill the SSM/I gaps. The figure also reveals the high sensitivity of MERIS for small-scale variations in the water vapour field, such as visible over Western Turkey.

### 4.2 Monthly means

The monthly mean water vapour over land in each grid box is calculated from the average of all available daily values. The resulting monthly mean over land and coastal ocean can be regarded as the cloud-free, forenoon monthly average of TCWV. Similar to the daily uncertainties, the associated uncertainty of the monthly mean value is





ESSDD
7, 59–88, 2014



derived from the average uncertainty of the contributing daily values. Again, the standard deviation among the daily values is provided in addition to reflect the temporal variability of TCWV during the course of the month.

The average of all swath-based SSM/I retrievals build the monthly mean TCWV over ocean. Accordingly, a standard deviation is provided based on the same swath-based data points, whose associated uncertainty measures are averaged to build a monthly mean uncertainty representative for each grid box.

Exemplarily, Fig. 3 shows the global distribution of monthly mean TCWV for January and June 2003 and the associated uncertainty for both months. Over ocean, the absolute uncertainty follows the general distribution of TCWV and is in the region of 5 % in the tropics and mid latitudes. Over coastal waters, where the monthly averaged TCWV is based on MERIS measurements, the uncertainty is increased (see for instance Adriatic Sea, Caspian Sea or the Aegean). Over land, the uncertainty can exceed 10 % in regions with strong cloud contamination, such as found in the ITCZ region. Over highly reflective surfaces, such as desert or snow regions, the uncertainty is strongly reduced. The number of single observations used for the generation of the monthly mean values is shown in the bottom panels. While over ocean an almost constant sampling is achieved, over land the number of valid observations is strongly affected by the presence of clouds.

## 5 Validation

### 5.1 Validation against independent datasets

The individual, swath-based level 2 retrievals of MERIS and SSM/I were thoroughly validated against a number of ground-based reference data sets. In case of MERIS, Lindstrot et al. (2012) overall reported a globally small wet bias ($\approx 1\,\mathrm{kg\,m^{-2}}$) and bias-corrected root mean square deviations (rmsd) of $3.7\,\mathrm{kg\,m^{-2}}$ (global Aeronet sun photometer measurements), $2.7\,\mathrm{kg\,m^{-2}}$ (global GUAN radiosondes), $1.3\,\mathrm{kg\,m^{-2}}$ (ARM site





ESSDD
7, 59–88, 2014



microwave radiometer measurements) and 2.1 $kg\,m^{-2}$ (German ground-based GPS data), based on analysing all available collocations within the years 2003 to 2005. The MERIS retrieval algorithm can therefore be regarded as of high accuracy and precision. In case of SSM/I, Fig. 4 shows a comparison against the ground-based microwave radiometer measurements taken at the Nauru ARM site between 1998 and 2008. Here, a distance of less than 1° between the ARM site and a SSM/I footprint, completely covering ocean surfaces, was the collocation criterion. The bias and the bias-corrected rmsd of −0.48 $kg\,m^{-2}$ and 1.8 $kg\,m^{-2}$, respectively reveal the high accuracy and precision of the SSM/I TCWV retrieval.

On level-3 basis, the complete 6 yr-spanning time series was evaluated by monitoring the bias and rmsd with respect to the GUAN radiosonde observations. The collocation contains pairs of SSM/I and GUAN as well as pairs of MERIS and GUAN data. However, the evaluation results will be dominated by the MERIS and GUAN pairs. Figure 5 shows the resulting time series of bias and rmsd, globally averaged over all GUAN stations. A small wet bias can be observed which is generally below 1 $kg\,m^{-2}$ but approaches 2 $kg\,m^{-2}$ for some months after 2006. The bias-corrected rmsd is between 4 and 5 $kg\,m^{-2}$ throughout the time series. Neither the bias nor the standard deviation exhibit any seasonal signal. Figure 6 shows the scatterplot of SSM/I-MERIS and GUAN monthly mean TCWV values, generated by using all individual GUAN stations for the complete 6 yr time series, resulting in 5492 collocations. In agreement with the findings shown in Fig. 5, the rmsd is around 4.4 $kg\,m^{-2}$, with a small wet bias of 0.7 $kg\,m^{-2}$. The ocean collocations seem to exhibit a slightly higher bias. Despite of general limits of comparing spaceborne observations to radiosonde measurements, these findings indicate a generally high accuracy and precision of the SSM/I-MERIS TCWV dataset.

### 5.2 Consistency between MERIS and SSM/I retrievals

In order to assess the presence of a potential bias between the retrieval algorithms, the MERIS TCWV retrieval was applied to cloud-free ocean areas exhibiting a significant





ESSDD
7, 59–88, 2014



fraction of directly reflected sun light. In contrast to measurements over the dark ocean, for sun glint geometries the sensitivity of the MERIS measurements to the full vertical column of water vapour is established by a signifant fraction of light being reflected at the lower boundary of the atmosphere. Due the ENVISAT forenoon orbit and the MERIS observation geometry, a significant amount of sun glint affected pixels appears in the Eastern part of the tropical and subtropical section of each orbit, provided that ocean pixels are present here.

In order to perform the scattering correction of MERIS measurements, the surface reflectance was calculated using the wind speed for parametrizing the sea surface roughness (Cox and Munk, 1954; Koepke, 1984). Afterwards, the retrieval is performed in the same way as over land, except for the estimation of AOT which is set to 0.1 in the inner part of the sun glint areas.

There are two difficulties to be noted for the comparison of SSM/I and MERIS retrievals over ocean:

1. For the MERIS retrieval, the same scattering correction factors as over land are used, calculated based on the assumption of a Lambertian surface. Since this assumption over ocean is inappropriate, increased uncertainties are to be expected.
2. The observation time difference of two to four hours potentially introduces a bias.
3. While MERIS is a clear sky-only retrieval, SSM/I retrievals are performed under all sky conditions, except for heavily precipitating regions.

One month (July 2007) of MERIS TCWV retrievals over open ocean were used to compare to SSM/I retrievals. In order to compensate for the differing footprint sizes and observation times, the comparison was performed on a 0.5° grid. Figure 7 shows a zoom into the Atlantic Ocean for measurements of SSM/I and MERIS on 9 July 2007, as well as the ocean surface reflectance for the MERIS viewing geometry. As expected, both retrievals show a rather high agreement for most of the sun glint areas, shown as unshaded elliptic regions, while larger deviations can be found over the dark ocean, shown as shaded regions.





ESSDD
7, 59–88, 2014



Figure 8 shows the resulting difference of the two retrievals ($TCWV_{MERIS} - TCWV_{SSM/I}$) as a function of the ocean surface reflectance, based on analysing one complete month of collocated measurements. A large bias of MERIS TCWV is found for dark ocean surfaces, hinting at a not properly working scattering correction scheme. The bias decreases with increasing ocean surface reflectance (and scattering becomes less important), with values below 1 $kg\,m^{-2}$ and a Pearson product-moment correlation coefficient around 0.85 for reflectances higher than 0.15. Despite of the above limitations of the comparisons of both retrievals, this hints at a high consistency among the two completely independent data sources.

## 6 Conclusions

The ESA DUE GlobVapour combined SSM/I-MERIS dataset of total columnar water vapour in its current version spans the years 2003 to 2008 and consists in daily composites of MERIS forenoon TCWV observations over cloud-free land and coastal ocean and SSM/I all-sky morning observations over ocean, as well as monthly averages. The data set is available in a high resolution ($0.05^\circ \times 0.05^\circ$) and at a coarse resolution version ($0.5^\circ \times 0.5^\circ$). To provide consistent resolution, SSM/I is oversampled in the former case and MERIS is averaged in the latter case.

The validation studies showed high agreements with GUAN radiosonde data of water vapour, with a weak wet bias of 0.74 $kg\,m^{-2}$ and a standard deviation of 4.4 $kg\,m^{-2}$. Furthermore, the SSM/I-MERIS time series is free of seasonal biases. By applying the MERIS retrieval algorithm to ocean areas, the consistency of the two data sources could be verified. Over sun glint regions, where the MERIS TCWV retrieval is of similar quality as over land, only a small positive bias of MERIS TCWV with respect to SSM/I retrievals was found. However, it is important to note that the limitation to clear sky scenes over land might introduce an inconsistency with respect to the all-sky retrievals over ocean as described e.g. in Mieruch et al. (2010). The combination of both data sources was carried out such that the individual properties of the microwave





ESSDD
7, 59–88, 2014



and near-infrared products, in particular their uncertainties, were not modified and are therefore well defined. Due to its known and defined quality, its global coverage and spatial consistency as well as its high spatial resolution over land, this unique data set enables climate and process studies on both land and ocean. The SSM/I-MERIS TCWV data set is freely available at www.globvapour.info.

An extension of the data set is possible to cover at least the full ENVISAT lifetime (2002–2012). With respect to future satellite missions, the upcoming Ocean and Land Colour Instrument (OLCI) onboard the Sentinel-3 satellites, flying in an ENVISAT-like orbit with the same equator crossing time, will provide similar measurements in the near infrared water vapour absorption band (Diedrich et al., 2013). With respect to the SSM/I instrument, it is currently foreseen to extend the SSM/I series at least into the 2020s and with the microwave imager instrument (MWI) planned to be deployed onboard the Eumetsat Polar System–Second Generation (EPS-SG) satellites allowing to further extend SSM/I-type measurements into the 2030s. The combined data set presented here could therefore be a demonstrator for a potential future time series covering at least a few decades of water vapour observations over land and ocean.

*Acknowledgements.* This work was performed in the framework of the ESA DUE GlobVapour project (ESA contract number 22696/09/I-OL). The NWP SAF is kindly acknowledged for providing the SSM/I 1D-Var software package. The CM SAF kindly provided an inter-calibrated SSM/I data set.

## References

Alishouse, J. C., Snyder, S. A., Jennifer, V., and Ferraro, R. R.: Determination of oceanic total precipitable water from the SSM/I, IEEE T. Geosci. Remote, 28, 811–816, 1990. 65

Andersson, A., Fennig, K., Klepp, C., Bakan, S., Graßl, H., and Schulz, J.: The Hamburg Ocean Atmosphere Parameters and Fluxes from Satellite Data – HOAPS-3, Earth Syst. Sci. Data, 2, 215–234, doi:10.5194/essd-2-215-2010, 2010. 65, 68





ESSDD

7, 59–88, 2014



Bennartz, R. and Fischer, J.: A modified *k*-distribution approach applied to narrow band water vapour and oxygen absorption estimates in the near infrared, J. Quant. Spectrosc. Ra., 66, 539–553, 2000. 67

Cox, C. and Munk, W.: Measurement of the roughness of the sea surface from photographs of the Sun's glitter, J. Opt. Soc. Am., 44, 838–850, 1954. 74

Deblonde, G.: NWP SAF User's Guide: Standalone 1D-var scheme for the SSM/I, SSMIS and AMSU, NWPSAF-MO-UD-001 Version 1.0, 2001. 68

Delwart, S., Preusker, R., Bourg, L., Santer, R., Ramon, D., and Fischer, J.: MERIS inflight spectral calibration, Int. J. Remote Sens., 28, 479–496, 2007. 66

Diedrich, H., Preusker, R., Lindstrot, R., and Fischer, J.: Quantification of uncertainties of water vapour column retrievals using future instruments, Atmos. Meas. Tech., 6, 359–370, doi:10.5194/amt-6-359-2013, 2013. 76

Fell, F. and Fischer, J.: Numerical simulation of the light field in the atmosphere-ocean system using the matrix-operator method, J. Quant. Spectrosc. Ra., 3, 351–388, 2001. 67

Forster, P. D. F. and Collins, M.: Quantifying the water vapour feedback associated with post-Pinatubo cooling, Clim. Dynam., 23, 207–214, 2004. 61

Hollinger, J. P.: DMSP Special Sensor Microwave Imager Calibration/Validation, NRL Final Rep., vol. I, Tech. rep., Nav. Res. Lab., Washington, DC, 1991. 65

Hollstein, A. and Fischer, J.: Radiative transfer solutions for coupled atmosphere ocean systems using the matrix operator technique, J. Quant. Spectrosc. Ra., 113, 536–548, doi:10.1016/j.jqsrt.2012.01.010, 2012. 67

Kiehl, J. and Trenberth, K. E.: Earth's annual global mean energy budget, B. Am. Meteorol. Soc., 78, 197–208, 1997. 61

Koepke, P.: Effective reflectance of oceanic whitecaps, Appl. Optics, 23, 1816–1824, 1984. 74

Lindstrot, R., Preusker, R., and Fischer, J.: The empirical correction of stray light in the MERIS oxygen A band channel, J. Atmos. Ocean. Tech., 27, 1185–1194, 2010. 66

Lindstrot, R., Preusker, R., Diedrich, H., Doppler, L., Bennartz, R., and Fischer, J.: 1D-Var retrieval of daytime total columnar water vapour from MERIS measurements, Atmos. Meas. Tech., 5, 631–646, doi:10.5194/amt-5-631-2012, 2012. 67, 72

MERIS Quality Working Group: MERIS 3rd data reprocessing, Software and ADF updates, Tech. Rep. A879.N T.008.ACRI-ST, ACRI, available at: http://earth.eo.esa.int/pcs/envisat/meris/documentation/ (last access: 9 January 2014), 2011. 64





ESSDD

7, 59–88, 2014



Mieruch, S., Schröder, M., Noël, S., and Schulz, J.: Comparison of monthly means of global total column water vapor retrieved from independent satellite observations, J. Geophys. Res., 115, D23310, doi:10.1029/2010JD013946, 2010. 75

O'Gorman, P. A. and Muller, C. J.: How closely do changes in surface and column water vapor follow Clausius–Clapeyron scaling in climate change simulations?, Environ. Res. Lett., 5, 7 pp., 2010. 61

Phalippou, L.: Variational retrieval of humidity profile, wind speed and cloud liquid-water path with the SSM/I: potential for numerical weather prediction, Q. J. Roy. Meteor. Soc., 122, 327–355, 1996. 65, 68

Pougatchev, N., August, T., Calbet, X., Hultberg, T., Oduleye, O., Schlüssel, P., Stiller, B., Germain, K. St., and Bingham, G.: IASI temperature and water vapor retrievals – error assessment and validation, Atmos. Chem. Phys., 9, 6453–6458, doi:10.5194/acp-9-6453-2009, 2009. 62

Preusker, R. and Lindstrot, R.: Remote sensing of cloud-top pressure using moderately resolved measurements within the oxygen A band – a sensitivity study, J. Appl. Meteorol. Clim., 48, 1562–1574, 2009. 66

Randel, D. L., Vonder Haar, T. H., Ringerud, M. A., Stephens, G. L., Greenwald, T. J., and Combs, C. L.: A new global water vapor dataset, B. Am. Meteorol. Soc., 77, 1233–1246, 1996. 63

Rast, M., Bezy, J. L., and Bruzzi, S.: The ESA Medium Resolution Imaging Spectrometer MERIS – a review of the instrument and its mission, Int. J. Remote Sens., 20, 1681–1702, 1999. 64

Rodgers, C.: Inverse Methods for Atmospheric Sounding: Theory and Practice, World Scientific, London, 2000. 68

Rothman, L., Gordon, I., Barbe, A., Benner, D., Bernath, P., Birk, M., Boudon, V., Brown, L., Campargue, A., Champion, J.-P., Chance, K., Coudert, L., Dana, V., Devi, V., Fally, S., Flaud, J.-M., Gamache, R., Goldman, A., Jacquemart, D., Kleiner, I., Lacome, N., Lafferty, W., Mandin, J.-Y., Massie, S., Mikhailenko, S., Miller, C., Moazzen-Ahmadi, N., Naumenko, O., Nikitin, A., Orphal, J., Perevalov, V., Perrin, A., Predoi-Cross, A., Rinsland, C., Rotger, M., Simeckova, M., Smith, M., Sung, K., Tashkun, S., Tennyson, J., Toth, R., Vandaele, A., and Auwera, J. V.: The HITRAN 2008 molecular spectroscopic database, J. Quant. Spectrosc. Ra., 110, 533–572, doi:10.1016/j.jqsrt.2009.02.013, 2009. 67





ESSDD
7, 59–88, 2014



Schlüssel, P. and Emery, W. J.: Atmospheric water vapour over oceans from SSM/I measurements, Int. J. Remote Sens., 11, 753–766, doi:10.1080/01431169008955055, 1990. 65, 68

Schröder, M., Jonas, M., Lindau, R., Schulz, J., and Fennig, K.: The CM SAF SSM/I-based total column water vapour climate data record: methods and evaluation against re-analyses and satellite, Atmos. Meas. Tech., 6, 765–775, doi:10.5194/amt-6-765-2013, 2013. 68

Schulz, J., Schluessel, P., and Grassl, H.: Water vapour in the atmospheric boundary layer over oceans from SSM/I measurements, Int. J. Remote Sens., 14, 2773–2789, doi:10.1080/01431169308904308, 1993. 65

Soden, B. J., Wetherald, R. T., Stenchikov, G. L., and Robock, A.: Global cooling after the eruption of Mount Pinatubo: a test of climate feedback by water vapor, Science, 296, 727–730, doi:10.1126/science.296.5568.727, 2002. 61

Susskind, J., Barnet, C. D., and Blaisdell, J. M.: Retrieval of atmospheric and surface parameters from AIRS/AMSU/HSB data in the presence of clouds, IEEE T. Geosci. Remote, 41, 390–409, 2003. 62

Trenberth, K. E. and Stepaniak, D. P.: Covariability of components of poleward atmospheric energy transports on seasonal and interannual timescales, J. Climate, 16, 3691–3705, 2003a. 61

Trenberth, K. E. and Stepaniak, D. P.: Seamless poleward atmospheric energy transports and implications for the Hadley Circulation, J. Climate, 16, 3706–3722, 2003b. 61

Trenberth, K. E., Fasullo, J., and Smith, L.: Trends and variability in column-integrated atmospheric water vapor, Clim. Dynam., 24, 741–758, doi:10.1007/s00382-005-0017-4, 2005. 61

Trenberth, K. E., Jones, P. D., Ambenje, P., Bojariu, R., Easterling, D., Klein Tank, A., Parker, D., Rahimzadeh, F., Renwick, J. A., Rusticucci, M., Soden, B., and Zhai, P.: Observations: Surface and Atmospheric Climate Change, in: Climate Change 2007: The Physical Science Basis. Contribution of Working Group I to the Fourth Assessment Report of the Intergovernmental Panel on Climate Change, edited by: Solomon, S., Qin, D., Manning, M., Chen, Z., Marquis, M., Averyt, K. B., Tignor, M., and Miller, H. L., Cambridge University Press, Cambridge, United Kingdom and New York, NY, USA, 2007. 61

Trenberth, K. E., Fasullo, J., and Kiehl, J.: Earth's global energy budget, B. Am. Meteorol. Soc., 90, 311–323, doi:10.1175/2008BAMS2634.1, 2008. 61

Vonder Haar, T. H., Bytheway, J. L., and Forsythe, J. M.: Weather and climate analyses using improved global water vapor observations, Geophys. Res. Lett., 39, L15802, doi:10.1029/2012GL052094, 2012. 63





ESSDD
7, 59–88, 2014



Wentz, F.: A well-calibrated ocean algorithm for special sensor microwave/imager, J. Geophys. Res., 102, 8703–8718, 1997. 65, 68





ESSDD
7, 59–88, 2014



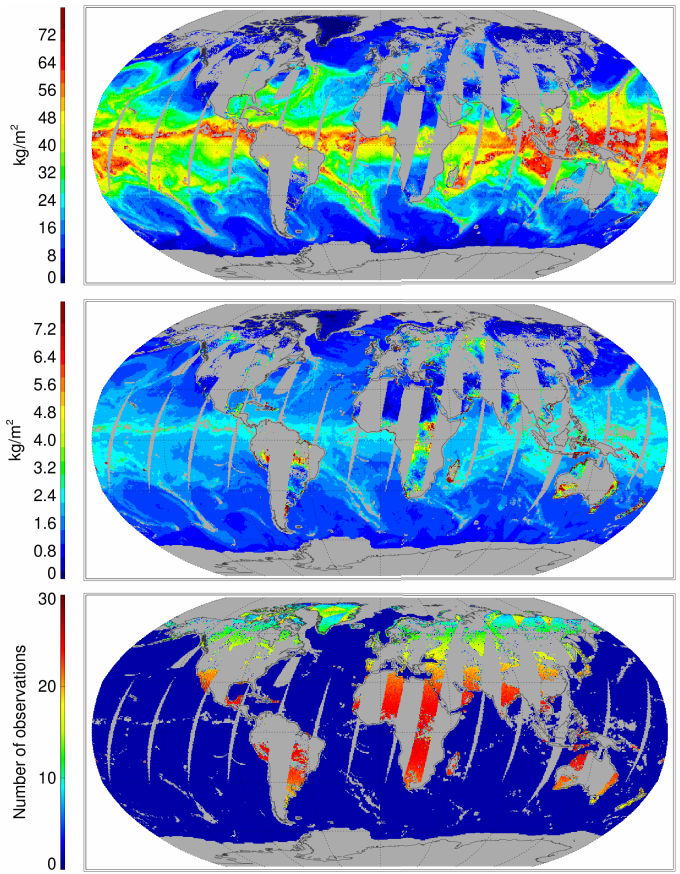


**Fig. 1.** Exemplary daily composite of TCWV (top), associated uncertainty (middle) and number of observations used (10 May 2003).





ESSDD
7, 59–88, 2014



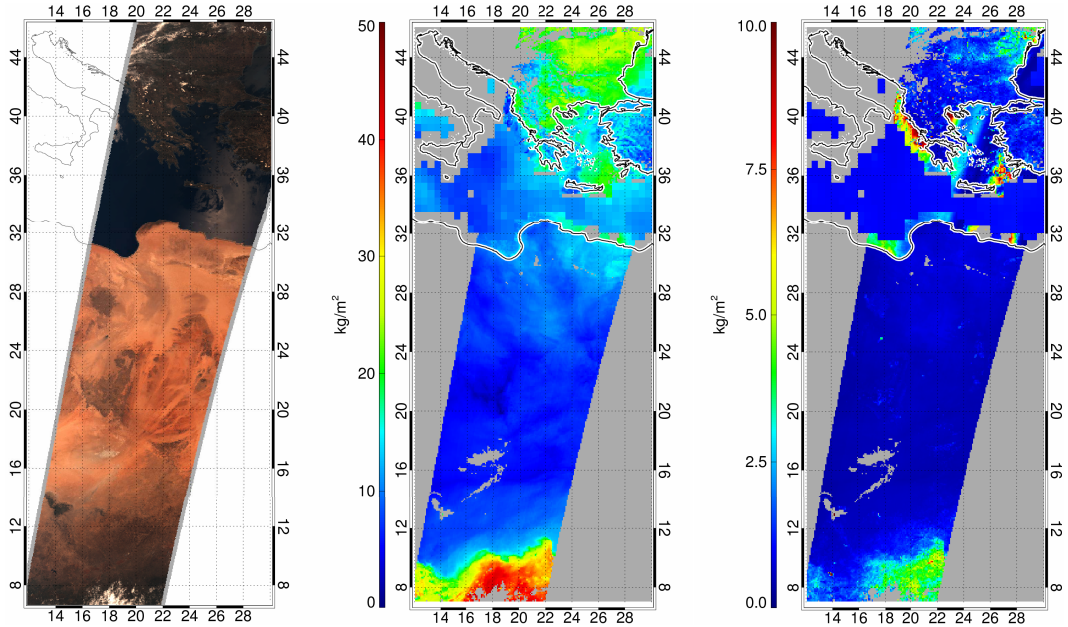


**Fig. 2.** MERIS RGB image of scene over Mediterranean Sea from 2 May 2003 (left) and zoom into daily composite of TCWV (middle) and uncertainty of TCWV (right) from MERIS and SSM/I measurements.





ESSDD
7, 59–88, 2014



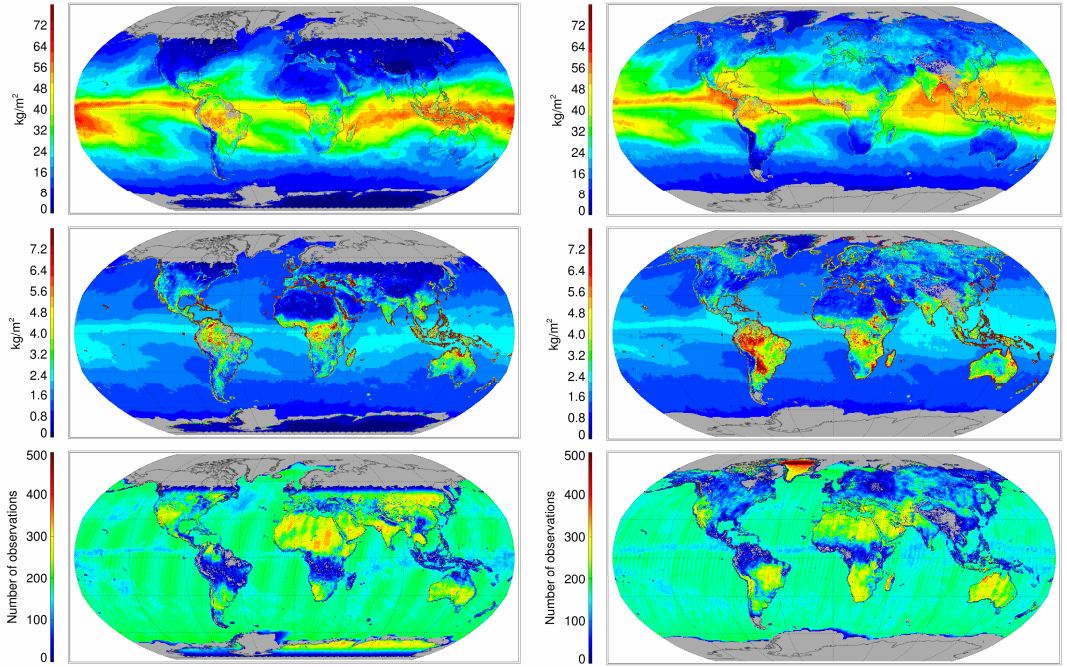


**Fig. 3.** Monthly mean TCWV (top), associated uncertainty (middle) and number of observations used (bottom) for January (left) and June (right) 2003.





ESSDD
7, 59–88, 2014



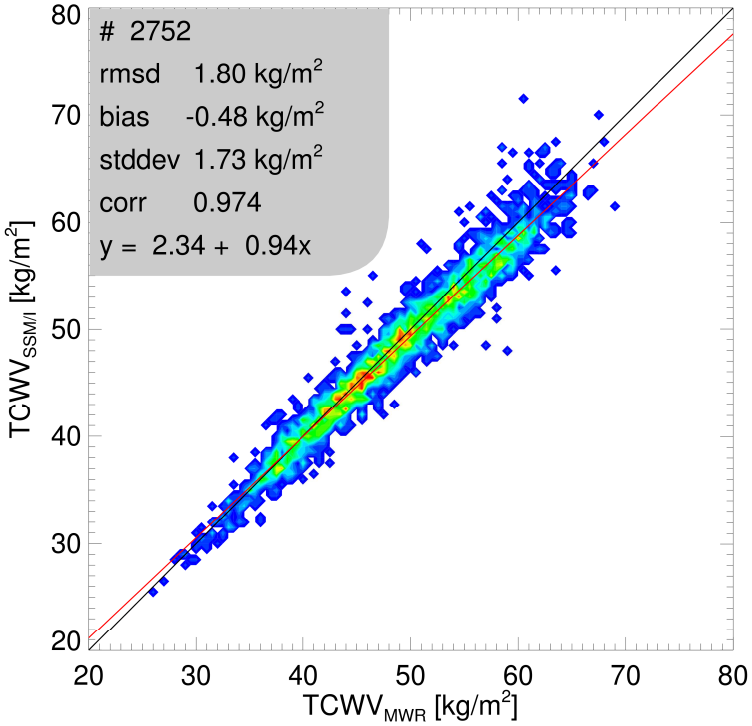


**Fig. 4.** Normalized frequency of occurrence for comparison of SSM/I-derived TCWV against ARM Nauru microwave radiometer data for the period 1998–2008. Relative frequency of occurrence is shown in colour with blue indicating low frequency and red high frequency of occurrence. Top left box specifies sample size, root mean square deviation, bias, standard deviation and offset and slope of linear best fit.





ESSDD
7, 59–88, 2014



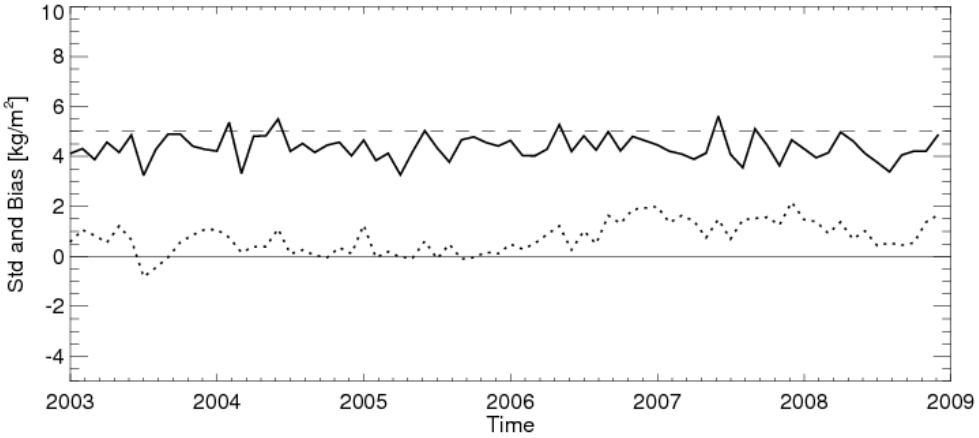


**Fig. 5.** Time series of bias (dotted) and bias-corrected rmsd (solid) of SSM/I-MERIS monthly mean TCWV with respect to GUAN, averaged over all GUAN stations.





ESSDD
7, 59–88, 2014



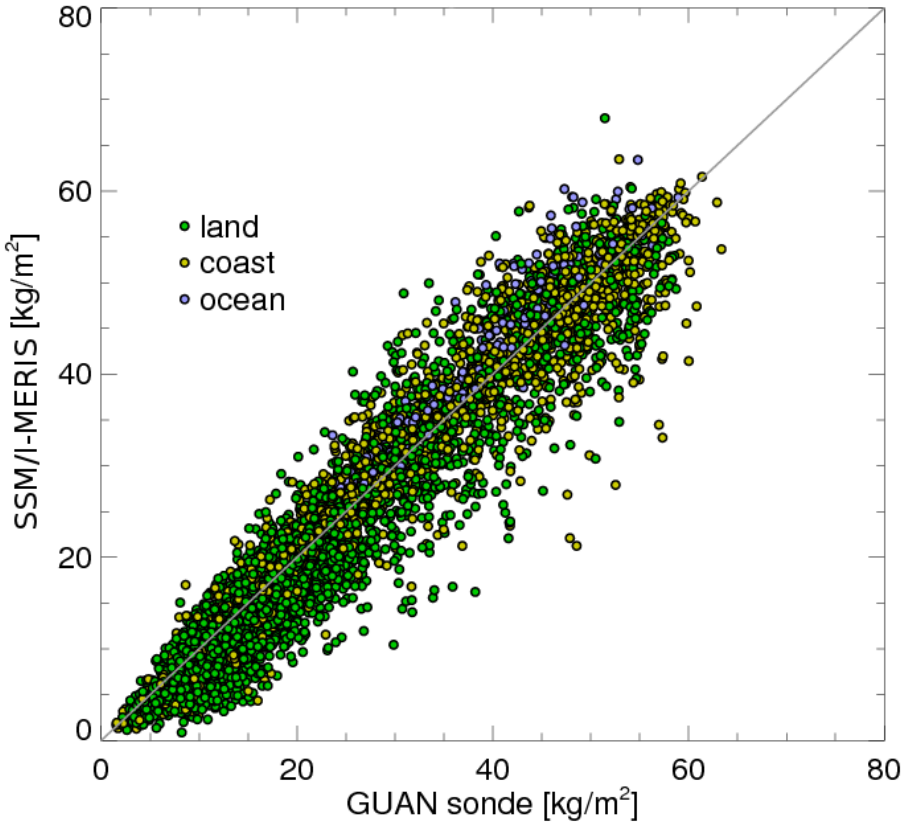


**Fig. 6.** Scatterplot of SSM/I-MERIS monthly mean TCWV vs. individual GUAN stations for the period 2003–2009 (5492 collocations). Resulting root mean square deviation is 4.4 kg m$^{-2}$, bias is 0.7 kg m$^{-2}$.





ESSDD
7, 59–88, 2014



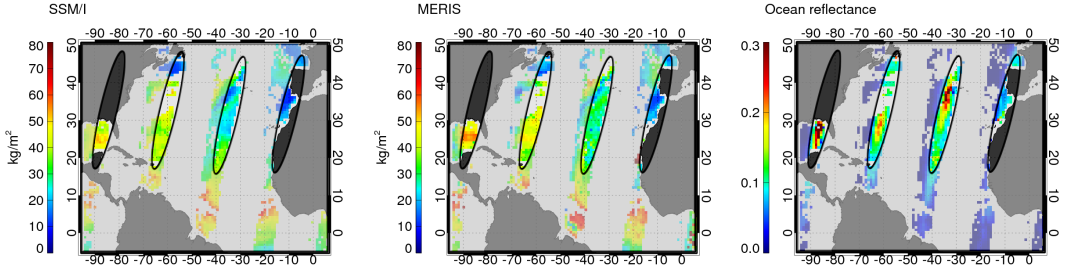


**Fig. 7.** Zoom into daily composites of TCWV from SSM/I (left) and MERIS (middle) over ocean and ocean surface reflectance at 900 nm for MERIS viewing geometry (right). Plots only show data where both MERIS and SSM/I retrievals are valid. Unshaded elliptic areas indicate regions where MERIS retrieval is reliable.





ESSDD
7, 59–88, 2014



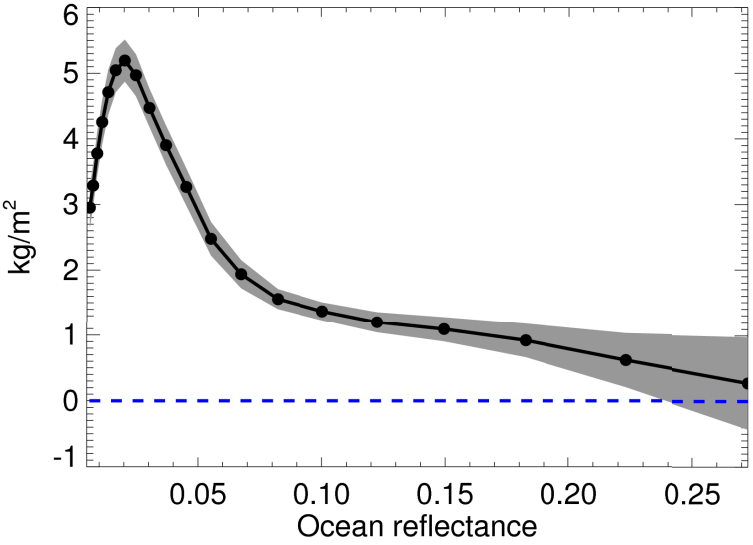


**Fig. 8.** Difference of MERIS TCWV and SSM/I TCWV over ocean (MERIS – SSM/I) as a function of ocean surface reflectance, analyzed from one month of collocated MERIS and SSM/I observations (July 2007). Grey shaded area indicates standard deviation of bias, analyzed from bootstrapping statistics.





ESSDD
7, 59–88, 2014